Spectroscopy 17 (2003) 169–181
IOS Press

NMR structural analysis of vascular endothelial growth factor in complex with a phage-derived peptide antagonist

Borlan Pan and Wayne J. Fairbrother *
Department of Protein Engineering, Genentech, Inc., South San Francisco, CA 94080, USA

Abstract. Vascular endothelial growth factor (VEGF) is a covalently linked homodimeric protein that functions as an endothelial cell-specific mitogen, and is an important mediator of pathological angiogenesis. Phage display has been used to select three different classes of novel disulfide-constrained peptides that bind to VEGF and disrupt receptor binding with IC_{50} values between 0.2–10 μM. Mapping of peptide induced nuclear magnetic resonance (NMR) chemical shift changes shows that they target a region of the VEGF receptor-binding domain that overlaps with the contact surfaces of the receptors, Flt-1 and KDR. The structure of one of these 28-kDa VEGF/peptide complexes was determined by NMR spectroscopy. The structure is based on a total of 4416 internuclear distance and dihedral angle restraints derived from data obtained using samples of the complex containing either $^{13}C/^{15}N$-labeled peptide or protein. Incorporation of residual dipolar coupling restraints improved both the precision and accuracy of the structure (as judged by comparison with crystal structures of VEGF). Comparison with the structure of a different VEGF/peptide complex reveals different peptide binding modes that each resemble those of natural protein ligands (an anti-VEGF antibody and the VEGF-receptor Flt-1). Prospects for the development of small-molecule antagonists of VEGF, based on the VEGF-bound peptide structures, are discussed.

1. Introduction

Vascular endothelial growth factor (VEGF) is a covalently linked homodimeric member of the cystine-knot family of growth factors [1]. VEGF functions as an endothelial cell-specific mitogen and is a primary regulator of physiological vasculogenesis and angiogenesis [2]; it is also an important mediator of pathological angiogenesis associated with a variety of disease states including cancer, rheumatoid arthritis, and proliferative retinopathy [3]. In particular, VEGF mRNA is upregulated in many tumor types [4,5] suggesting that antagonists of VEGF may have significant clinical benefits. Indeed, inhibition of VEGF activity has been shown to suppress the growth of a wide variety of tumors in murine models [5–7], and clinical trials of a humanized neutralizing monoclonal antibody [8] in cancer patients are ongoing.

Six different isoforms of VEGF are expressed in humans having 121, 145, 165, 183, 189, or 206 residues per monomer [2]. Each of the different isoforms share a common N-terminal receptor-binding domain, while the longer isoforms ($VEGF_{165}$, $VEGF_{183}$, $VEGF_{189}$, and $VEGF_{206}$) also include a C-terminal heparin-binding domain [9,10]. VEGF signaling is mediated via dimerization of its tyrosine kinase receptors, Flt-1 (*fms*-like tyrosine kinase; VEGFR-1) and KDR (kinase-insert domain receptor; VEGFR-2), using a pair of identical receptor-binding sites localized at the poles of the dimeric VEGF receptor-binding domain [1,11–14]. KDR, the lower affinity receptor ($K_d \sim$ 75–125 pM) [15], is the primary signaling receptor of VEGF and its activation is sufficient to stimulate vascular endothelial cell mitogenesis [16], while the higher affinity receptor Flt-1 ($K_d \sim$ 10–20 pM) [17] is thought to function,

*Corresponding author. Tel.: +1 650 225 6372; Fax: +1 650 225 3734; E-mail: fairbro@gene.com.

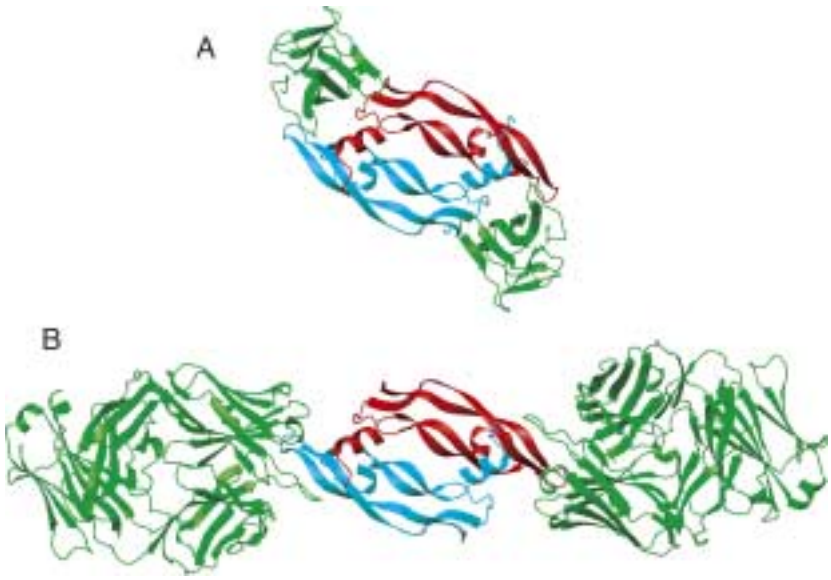

Fig. 1. (A) Crystal structure of the VEGF–Flt-1_{D2} complex (PDB accession code 1FLT). (B) Crystal structure of VEGF in complex with the Fab fragment of a neutralizing antibody (PDB accession code 1CZ8). The VEGF monomers are colored red and cyan, respectively, and the bound ligands are colored green. This figure was produced using the program MOLMOL [57].

at least in some circumstances, as a "decoy" receptor that is able to negatively regulate angiogenesis by sequestering VEGF [18,19].

A high-resolution crystal structure of the complex between the VEGF receptor-binding domain and the second Ig-like domain of Flt-1 (Flt-1_{D2}) shows in detail the mode of ligand–receptor interaction [12]. Briefly, two copies of the receptor bind symmetrically at opposite ends of the VEGF dimer, with each copy contacting both VEGF monomers (Fig. 1A). Overall, the interface is rather flat and predominantly hydrophobic in nature. The KDR-binding site on VEGF, identified using alanine-scanning mutagenesis, overlaps significantly with the observed Flt-1_{D2}-binding site [1,11–13]. The binding sites for several neutralizing antibodies have also been shown to overlap with the KDR- and Flt-1-binding sites on the VEGF receptor-binding domain (Fig. 1B) [1,20,21].

Herein, we discuss recent efforts to identify and structurally characterize novel peptide antagonists of VEGF. In particular we emphasize the use of nuclear magnetic resonance (NMR) spectroscopy as a tool for identifying the peptide-binding sites on the protein, via backbone chemical shift mapping, as well as for complete determination of the three-dimensional structure of one such protein–peptide complex. In other systems, small-molecule lead compounds have been designed based on mimicking the interactions found for small, constrained peptide antagonists. Prospects for the development of novel, small-molecule antagonists of VEGF, based on the interactions observed between the phage-derived peptide antagonists and the VEGF receptor-binding domain, are discussed.

2. VEGF-binding peptides

Phage display of naive peptide libraries was used recently to identify three classes of small disulfide-constrained peptides that each bind to VEGF and block its interaction with KDR, with IC_{50} values in the range 0.2–10 μM (Fig. 2) [22]. In contrast to results obtained for several other phage-derived peptide

		IC_{50} (μM)
Class 1		
v106	GERWCFDGPRAWVCGWEI-NH_2	7.0 ± 0.9
Class 2		
v108	RGWVEICAADDYGRCLTEAQ-NH_2	2.2 ± 0.1
Class 3		
v107	GGNECDIARMWEWECFERL-NH_2	0.6 ± 0.3

Fig. 2. Sequences of representative phage-derived VEGF-binding peptides. The IC_{50} values for v106 and v108 are from reference [22], while that for v107 represents an average value from references [22] and [36].

antagonists of protein–protein interactions [23–28], NMR analysis of the different classes of VEGF-binding peptides free in aqueous solution was either impossible, due to poor peptide solubility (Class 1), or showed that the peptides were essentially unstructured (Class 2) or poorly ordered and/or aggregated (Class 3) [22].

2.1. Identification of peptide-binding sites by NMR chemical shift mapping

Despite the fact that free peptide structures were not definable, the interaction sites of the peptides on VEGF were readily determined by mapping NMR chemical shift perturbations upon peptide binding using 2D ^{1}H–^{15}N HSQC spectra of uniformly ^{15}N-labeled VEGF receptor-binding domain ($VEGF_{11-109}$). Nearly complete backbone resonance assignments for the 23-kDa homodimeric $VEGF_{11-109}$ construct were determined previously using a suite of seven 3D triple-resonance experiments and a 0.5 mM (1 mM $VEGF_{11-109}$ monomers) sample of uniformly $^{13}C/^{15}N$-labeled protein at 500 MHz, pH 7.0, 45°C [29]; these assignments were confirmed and extended more recently using data collected at 800 MHz [30].

NMR chemical shifts are exquisitely sensitive to the local magnetic-shielding environments, including contributions in proteins from aromatic ring current effects, peptide bond anisotropy, electrostatic interactions, and hydrogen bonds. Ligand binding inevitably causes local environmental changes for nuclei in amino acids at the binding interface, resulting in measurable chemical shift changes. In the absence of significant conformational change, identification of perturbed resonances provides a simple means to identify qualitatively the interaction sites of both peptide–protein and protein–protein complexes [31–33].

As can be seen in Fig. 3A, the ^{1}H–^{15}N HSQC spectrum of $VEGF_{11-109}$ at 45°C changes significantly upon adding saturating amounts of the class 3 peptide v107. The locations of amino acids with cross-peaks that have significant chemical shift changes upon binding representatives of the three peptide classes are mapped onto the crystal structure of $VEGF_{8-109}$ in Figs 3B–D. The three different classes of phage-derived peptides each have binding sites that overlap significantly with both receptor- and antibody-binding sites and with each other. However, there are also some distinct differences between the binding sites. For instance, the highest affinity peptide v107 appears to have significant contacts with the N-terminal helix (α1) and β-strands β4 and β7 that are not observed for the class 2 peptide v108. On the other hand, v108 contacts the α2–β2 loop region, in contrast to both v106 and v107, and β-strand β6, that is not part of the v107-binding site.

3. Structural studies of the VEGF–peptide complexes

3.1. Crystal structure of the VEGF–v108 complex

A subsequent X-ray crystal structure of v108 in complex with $VEGF_{8-109}$ confirmed the peptide-binding site determined by NMR chemical shift mapping (Fig. 4A) [34]. The peptide was observed

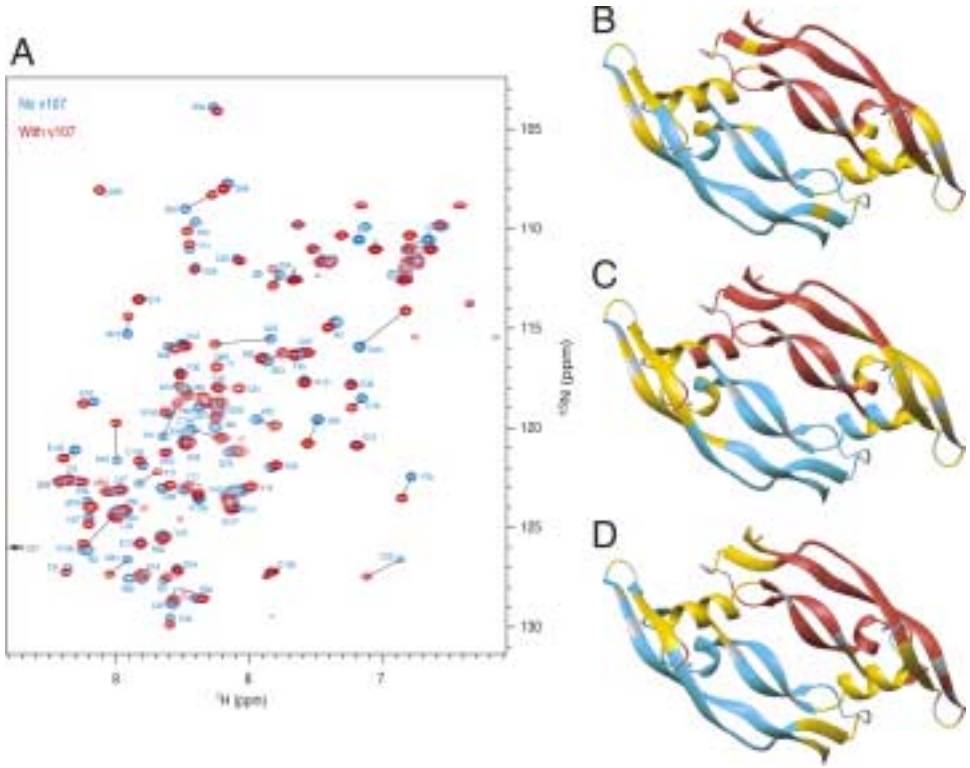

Fig. 3. (A) Superposition of 2D ^{1}H–^{15}N HSQC spectra of $VEGF_{11-109}$ in the absence (blue) and the presence (red) of the class 3 peptide v107. Cross peaks corresponding to the free protein are labeled. Peptide-binding induced shifts of selected cross peaks are indicated by lines. Schematic representations of the VEGF crystal structure illustrating in yellow the locations of amino acids experiencing significant chemical shift changes upon binding peptides v106 (B), v108 (C), and v107 (D); this figure was produced using the program MOLMOL [57].

to bind VEGF at the periphery of the Flt-1_{D2}-binding site, through primarily main-chain interactions mediated by the N-terminal six residues and residues in the disulfide loop. The C-terminal five residues of v108 do not contact VEGF, consistent with 1D ^{1}H-NMR spectra of the peptide that indicate that the C-terminal region of the peptide remains highly flexible in the protein–peptide complex (the methyl resonances of Thr17 and Ala19 remain sharp upon binding the protein, while those of Ala8 and Ala9 are considerably broadened, as expected for a peptide interacting with a 23-kDa protein). Truncation of the C-terminal four residues has been demonstrated to have a minimal effect on the affinity of v108 for VEGF [22,34].

Only 5 of the 13 VEGF residues in the interface with v108 are in contact with Flt-1_{D2} in the VEGF–receptor complex. However, 12 of these 13 VEGF residues also make intermolecular contacts in the VEGF–Fab complexes. Remarkably, the 20-residue peptide buries a total surface area of 1350 Å^2 on binding VEGF, or about 75% of the 1750–1800 Å^2 surface area buried by the considerably larger receptor-blocking Fabs. Furthermore, all VEGF atoms involved in conserved hydrogen-bonds in the v108 complex also form hydrogen-bonds with the Fabs (note that v108 does not bind in a unique conformation and that two slightly different sets of protein–peptide interactions are observed in the crystal structure of the complex). The binding mode of v108 therefore resembles most closely that of the anti-VEGF antibody rather than the receptor (*c.f.* Fig. 1). Indeed, only two hydrophobic side-chains from v108, Trp3 and

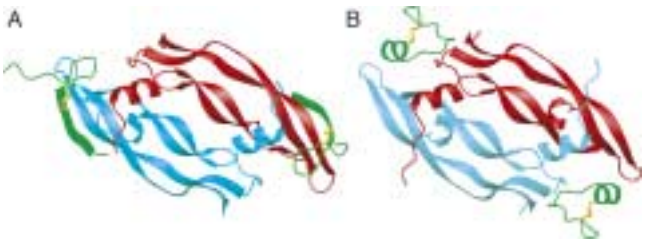

Fig. 4. (A) Crystal structure of the VEGF–v108 complex (PDB accession code 1VPP). (B) Representative solution structure of the VEGF–v107 complex taken from the ensemble of 24 structures (PDB accession code 1KAT). The VEGF monomer are colored red and cyan, respectively, and the bound peptide ligands are colored green, with the disulfide linkages shown as yellow bonds. This figure was produced using the program MOLMOL [57].

Ile6, have significant contacts with VEGF and these contacts lie outside the receptor-binding site. Therefore, because of its extended main-chain-mediated binding mode and the absence of side-chain-mediated contacts within the receptor-binding site, the phage-derived peptide v108 was deemed to be unsuitable for structure-based design of small molecule antagonists of VEGF [34].

3.2. NMR structural analysis of VEGF–peptide complexes

Based on the peptide-binding sites deduced from chemical shift mapping (Fig. 3), the remaining two peptide classes have binding sites on VEGF that overlap more significantly with the receptor-binding site. Unfortunately, these peptides have not proved amenable to crystallographic analysis. We therefore undertook the characterization of the complexes between these peptides and the VEGF receptor-binding domain by NMR spectroscopy.

Preliminary experiments with synthetic peptides v106 and v107 and ^{15}N-labeled $VEGF_{11-109}$ showed that heteronuclear filtered NMR experiments do not have sufficient sensitivity to enable complete assignment of the peptide resonances in the protein–peptide complexes. As noted previously, the ∼23-kDa homodimeric VEGF receptor-binding domain has an overall rotational correlation time, τ_c, of ∼15 ns at 45°C, due to the anisotropic shape of the molecule as well as concentration dependent aggregation [29]. The larger linewidths (larger spin-spin relaxation rate constants) of the peptides in the protein-bound state result in decreased sensitivity for experiments that rely on small (<10 Hz) homonuclear ^{3}J scalar couplings for coherence transfer (such as heteronuclear-filtered TOCSY experiments). Therefore, in order to take advantage of the increased sensitivity afforded by triple-resonance NMR methods [35] ^{13}C/^{15}N-labeled peptides were produced in *Escherichia coli* as fusion proteins in which the dimerization domain of GCN4 was C-terminally modified to include a linker (GPGG), an enterokinase recognition site (DDDDK), and the sequence for the VEGF-binding peptide (v106 or v107) [36]. Briefly, the resulting fusion peptides were purified by size-exclusion chromatography and reverse-phase HPLC chromatography. The final peptide samples were produced subsequently by cleavage with enterokinase, followed by oxidation with potassium ferricyanide [36]. In both cases, the yield from four litres of expression culture was sufficient for a single NMR sample of the protein–peptide complex.

3.3. NMR analysis of the VEGF–v106 complex

Despite the fact that the free peptide v106 was poorly soluble, nearly complete backbone $^{1}H_N$, $^{13}C_\alpha$, and ^{15}N resonance assignments of uniformly ^{13}C/^{15}N-labeled v106 in complex with $VEGF_{8-109}$ were obtained at 35°C from analysis of 3D triple-resonance HNCA and HN(CO)CA spectra. Unfortunately,

the peptide sample succumbed to proteolysis during, or soon after, the acquisition of these spectra so further analysis was not possible. However, based on the $^{13}C_\alpha$ chemical shifts obtained for the VEGF-bound peptide we deduce that v106 adopts a β-hairpin conformation [37–39]. Indeed, v106 shares the ten-residue CX_2GPX_2WVC disulfide-cycle motif found in other phage-derived peptides known to adopt β-hairpin structures, including agonists and antagonists of the erythropoietin receptor [27,40,41], and antagonists of the high affinity IgE receptor [25]. In addition, the hydrophobic amino acids Phe6, Trp12, and Val13 of v106 occupy positions that have been shown to stabilize 10-residue disulfide-constrained β-hairpins [42–44]. However, even with the knowledge that v106 contains a disulfide-constrained β-hairpin structure, there is still insufficient information to determine, with any reasonable degree of certainty, how the peptide binds VEGF.

3.4. NMR analysis of the VEGF–v107 complex

The binding site for the highest affinity peptide, v107, overlaps most extensively with that of the receptor, Flt-1_{D2}, and thus characterization of its protein-bound conformation is of great interest. Nearly complete backbone resonance assignments of uniformly $^{13}C/^{15}N$-labeled v107 were obtained at 35°C, in both the free and $VEGF_{8-109}$-bound states, from analysis of 3D TROSY-HNCA, CBCA(CO)NH, and ^{15}N-edited NOESY-HSQC spectra acquired at 800 MHz. Side-chain resonance assignments were obtained through analysis of 3D HCCH-TOCSY and ^{13}C-edited NOESY-HSQC spectra. Comparison of ^{15}N-HSQC spectra of free and VEGF-bound v107 indicates that binding to VEGF induces significant structuring of the peptide; the spectrum of free v107 has limited spectral dispersion, characteristic of a disordered peptide, that increases considerably upon complex formation [36].

A second sample of protein–peptide complex, containing uniformly $^{13}C/^{15}N$-labeled $VEGF_{11-109}$ and unlabeled synthetic v107, was used for assignment of the protein resonances [30]. The backbone ^1H_N, ^{13}C, and ^{15}N resonances were assigned at 45°C through analysis of 3D HNCO, (HCA)CONH, HNCA, CBCA(CO)NH, and ^{15}N-edited NOESY-HSQC spectra acquired at either 600 or 800 MHz. Side-chain assignments were obtained from analysis of 3D HCCH-TOCSY, HBHA(CO)NH, HCC(CO)NH, and ^{13}C-edited NOESY-HSQC spectra.

Having completed the resonance assignments, the solution structure of the VEGF–v107 complex was determined using primarily distance restraints derived from heteronuclear-edited NOESY spectra and dihedral angle restraints obtained from ^1H, ^{15}N, $^{13}C'$, and $^{13}C_\alpha$ chemical shifts using the TALOS program [45]. Intermolecular distance restraints between v107 and VEGF were obtained from a ^{12}C-F_1-filtered,^{13}C-F_3-edited NOESY spectrum [46] of the $^{13}C/^{15}N$-labeled $VEGF_{11-109}$-unlabeled v107 sample in 100% D_2O. A total of 3940 NOE-derived distance restraints (1580 $\times 2$ intra-VEGF monomer; 158 $\times 2$ inter-VEGF monomer; 142 $\times$ 2 intra-v107; 90 $\times$ 2 intermolecular VEGF–v107) and 476 dihedral angle restraints (103 $\times$ 2 ϕ; 89 $\times$ 2 ψ; 46 $\times$ 2 χ_1) were used in calculation of the dimeric complex structure ($\sim$18.7 distance/dihedral angle restraints per residue). The NOE distance and dihedral angle restraints were supplemented by 176 hydrogen bond restraints, 146 residual dipolar coupling (RDC) restraints [47], $^{13}C_\alpha/^{13}C_\beta$ chemical shift restraints [48], symmetry distance restraints [49], and non-crystallographic symmetry restraints. An ensemble of structures was calculated using a simulated annealing protocol with restrained torsion angle dynamics [50] using the program CNX (Accelrys), as described in detail elsewhere [36]; the 24 structures with the lowest residual restraint violation energies were selected to represent the solution structure of the VEGF–v107 complex (PDB accession code 1KAT). A representative structure from the ensemble is illustrated in Fig. 4B, where it may be compared to the crystal structure of the VEGF–v108 complex (Fig. 4A).

The final ensemble of structures satisfies the experimental restraints very well, with no distance or dihedral angle restraint violations greater than 0.1 Å or 1.0°, respectively. The precision of the structure is also high. For residues 15–105 of the VEGF dimer the atomic RMS deviations for the backbone atoms (N, C_α, C′) with respect to the mean coordinates are 0.37 ± 0.07 Å. As observed previously for crystal structures of VEGF [51], several regions of the dimer in complex with v107 are less well ordered, including the N-terminal residues 11–14, the C-terminal residues 106–109, and loop residues 37–44, 63–66, and 83–91. For the well ordered regions of VEGF, the atomic RMS deviations of the backbone atoms with respect to the mean coordinates are 0.25 ± 0.04 Å. The atomic RMS deviations of backbone atoms from the peptide-binding region of VEGF and peptide residues 5–19 with respect to the mean coordinates are 0.27 ± 0.04 Å, indicating that the protein–peptide interface is also well defined.

3.5. Effects of RDC restraints on the precision and accuracy of the VEGF–v107 complex

The inclusion of RDC restraints was found to have a significant impact on the precision and overall conformation of the solution structure of VEGF in complex with v107 [36]. Residual $^1D_{\mathrm{NH}}$ dipolar couplings for both v107 and VEGF were determined by subtracting the $^1J_{\mathrm{NH}}$ scalar coupling constants, measured using isotropic samples of the complex, from the $^1J_{\mathrm{NH}} + {}^1D_{\mathrm{NH}}$ values obtained from complex samples aligned partially using ∼15 mg·ml^{-1} pf1 phage [52]; the $^1\mathrm{H_N}$–^{15}N splittings were measured under both isotropic and partially aligned conditions using 2D IPAP ^{1}H–^{15}N HSQC experiments [53]. The residual dipolar coupling between two nuclei is given by:

$$D(\theta, \phi) = D_{\mathrm{a}}\left\{(3\cos^2\theta - 1) + \frac{3}{2}R(\sin^2\theta\cos 2\phi)\right\}, \tag{1}$$

where R is the rhombicity defined as $D_{\mathrm{r}}/D_{\mathrm{a}}$; D_{a} and D_{r} are the axial and rhombic components of the alignment tensor given by $\frac{1}{3}[D_{zz} - (D_{xx} + D_{yy})/2]$ and $\frac{1}{3}[D_{xx} - D_{yy}]$, respectively; and θ and ϕ are the cylindrical coordinates describing the orientation of the internuclear vector in the principal axis system of the molecular alignment tensor [47]. The RDC data thus establish the orientation of internuclear vectors with respect to a molecular alignment tensor axis that provides a global reference frame [47,54].

In order to test the effect of RDC refinement on the structure of the VEGF–v107 complex, structures were calculated with and without inclusion of RDC restraints [36]. As expected, the RDC-refined structures agree considerably better with the experimental RDC restraints than the structures refined without these restraints (Fig. 5A). The ensemble of structures calculated with RDC restraints is also more precise, with backbone RMS deviations with respect to the mean for VEGF residues 15–105 about 40% lower than for the ensemble calculated without RDC restraints (0.37 ± 0.07 compared to 0.60 ± 0.14 Å). Localized superpositions on the peptide-binding region or the peptide, however, do not yield significant differences in precision, indicating that the NOE-derived distance and dihedral angle restraints are sufficient to define the local conformation but not the relative orientations of structurally distant regions of the protein. The limitations of the short-range NOE distance and dihedral angle restraints is highlighted by comparison of the global conformations of the VEGF structures calculated with and without RDC restraints (Fig. 5B). The VEGF structure calculated without RDC restraints is clearly more expanded, particularly in the loop regions, where relatively fewer distance restraints define the structure. Furthermore, the structure of VEGF calculated with the RDC restraints is in significantly better agreement with the high-resolution crystal structures of VEGF than the structure calculated without RDC restraints (Fig. 5B). Therefore, the long-range geometric information contained in the RDC restraints improves both the global precision and accuracy of the VEGF–v107 complex structure.

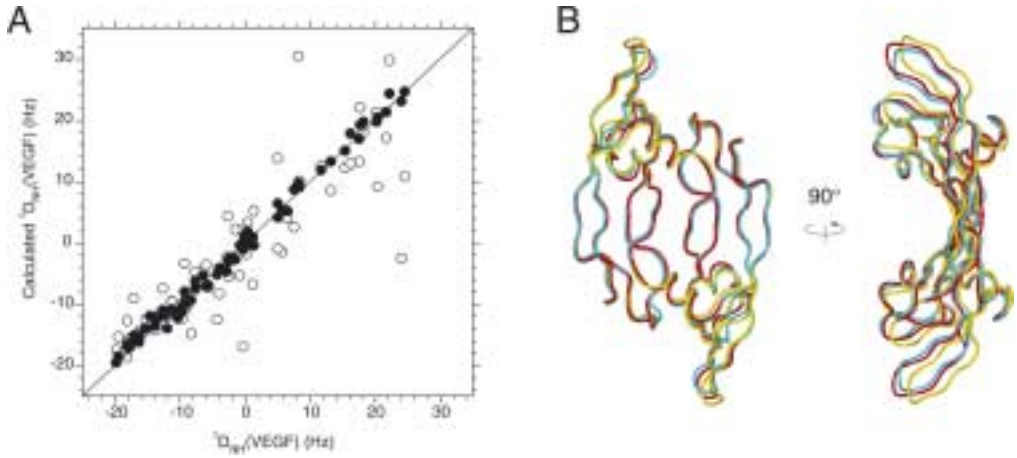

Fig. 5. (A) Correlation between experimental and calculated $^{1}D_{NH}$ for VEGF structures calculated with (filled) and without (open) RDC restraints. (B) Comparison of the mean structures of VEGF in complex with v107 calculated with (red) and without (yellow) RDC restraints and a high-resolution crystal structure of VEGF (cyan).

3.6. The VEGF–v107 interface

The VEGF-bound conformation of v107 consists of a disordered N-terminus (residues 1–4) followed by a type-I reverse turn (residues 6–9), an extended region (residues 9–12), and a well-defined C-terminal helix (residues 13–19) (Fig. 4B). The N-terminal four residues do not contact the protein, suggesting that a 15-residue peptide would be sufficient for binding. The peptide is strikingly amphipathic with the hydrophobic residues, that interact with VEGF, partitioned to one face (Fig. 6A). "Turn-helix" structures have been observed for several other phage-derived peptides, with each having a cluster of hydrophobic residues on one face that has been shown to be important for peptide structural stability and/or binding to their respective target proteins [23,24,28,55].

The v107-binding site on VEGF is in good agreement with that deduced by NMR chemical shift mapping, and as predicted, comparison of the VEGF–v107 and VEGF–Flt-1_{D2} complex structures shows that both ligands bind to similar regions at the poles of the VEGF dimer; the binding interfaces of these complexes are compared in Fig. 6. In both complexes, the interactions are mediated through predominantly hydrophobic side-chain contacts with nearly the same residues of VEGF in the interface. Inspection of Fig. 6 shows, however, that although v107 binds the same site on VEGF as Flt-1_{D2} it generally uses different amino acid residues. Despite these differences, the conserved hydrophobic nature of the v107 interaction with VEGF resembles that of the receptor more than the anti-VEGF antibody. In this case the 19-residue peptide v107 buries 1167 Å^2 of hydrophobic binding surface, or about 70% of the 1672 Å^2 total surface area buried by the 101-residue Flt-1_{D2}.

Functional characterization of the VEGF–v107 interface was achieved by alanine scanning both contact surfaces [36]. Comparison of the functional epitopes on VEGF for binding to v107 or Flt-1_{D2} reveals some differences, but also indicates that peptide and receptor binding require similar numbers of functionally important residues (Fig. 7). Important v107-binding determinants include Tyr21, Tyr25, Lys48, Leu66, Met81, and Met83, while the most important Flt-1_{D2}-binding determinants include Phe17, Met18, Tyr21, Gln22, Tyr25, and Leu66. Thus, although the structural epitope for v107 binding is ∼30% smaller

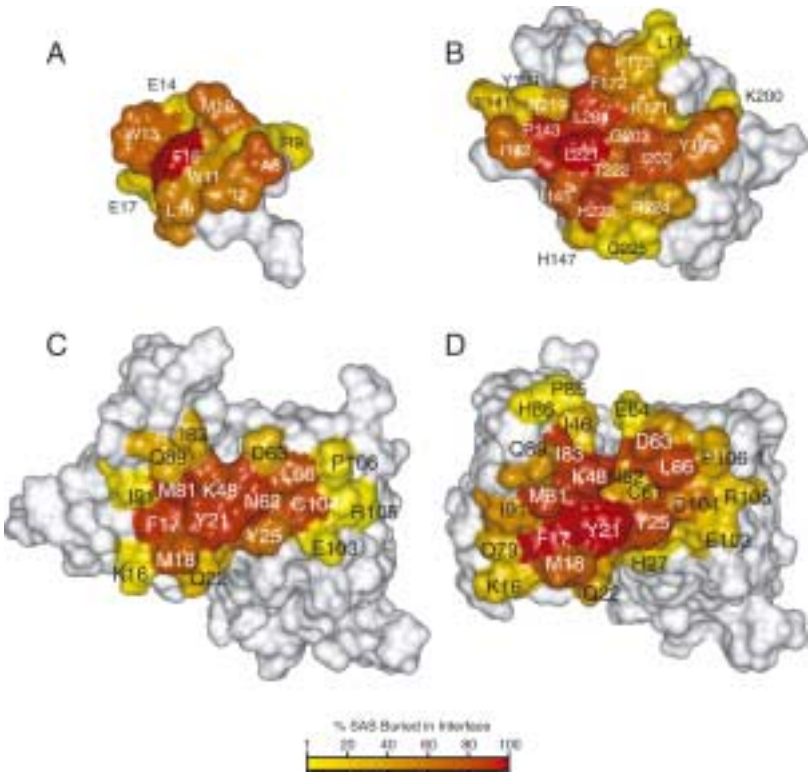

Fig. 6. Comparison of the binding interfaces of (A) v107 and (B) Flt-1_{D2} in complex with VEGF and the binding interfaces of VEGF in complex with (C) v107 and (D) Flt-1_{D2}. Surface amino acids are colored according to the percentage of solvent accessible surface (SAS) area buried in the interfaces on complex formation as indicated in the legend. The total surface area buried by each side of the respective interfaces are 622 (A), 810 (B), 545 (C), and 862 Å^2(D).

than that of Flt-1_{D2}, the functional epitopes are approximately the same size, suggesting that transfer of this novel peptide epitope to a potent small molecule scaffold might be difficult.

An alanine scan of the hydrophobic residues that constitute the structural binding epitope of v107 revealed that Met10, Trp11, Trp13, and Phe16 are critical for binding to VEGF. However, the sum of the individual side-chain contributions ($\Delta\Delta G_{\mathrm{Ala-wt}} \geqslant 18$ kcal·mol^{-1}) is significantly greater than the total binding energy ($\Delta G \approx -8$ kcal·mol^{-1}), suggesting that cooperativity exists between peptide binding and structural stabilization. In particular, Trp11 and Phe16 of v107 have significant intramolecular interactions. Substitution of these amino acids with alanine results in >2,000-fold losses in binding affinity for VEGF, with a substantial fraction of this loss likely resulting from destabilization of the bound peptide conformation. Unfortunately, there is no way to check the structural consequences of the alanine substitutions on the free peptide, as has been done for variants of other phage-derived peptides [24,25, 56], because v107 lacks a definable structure in the absence of VEGF. However, such non-additivity in the effects of alanine substitutions appears to be common amongst phage-derived peptides (at least in the limited number of cases in which such data are reported) [24–26,56], suggesting that cooperativity between structural and protein-binding determinants might be an inevitable consequence of minimizing a protein scaffold to a peptide scaffold.

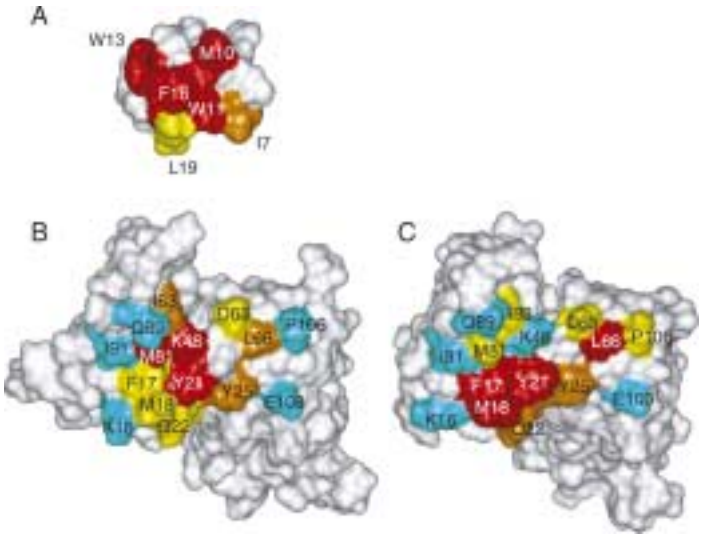

Fig. 7. Comparison of alanine scanning data for (A) v107 binding to VEGF, (B) VEGF binding to v107, and (C) VEGF binding to Flt-1_{D2}. Residues are colored according to the relative IC_{50} values of their respective alanine mutants as follows: red, >30-fold increase ($\Delta\Delta G_{\text{Ala-wt}} > 2.0$ kcal·mol^{-1}); orange, 10–30-fold increase (1.3 kcal·mol^{-1} $< \Delta\Delta G_{\text{Ala-wt}} <$ 2.0 kcal·mol^{-1}); yellow, 3–10-fold increase (0.6 kcal·mol^{-1} $< \Delta\Delta G_{\text{Ala-wt}} <$ 1.3 kcal·mol^{-1}); cyan, <3-fold increase ($\Delta\Delta G_{\text{Ala-wt}} <$ 0.6 kcal·mol^{-1}).

4. Conclusion

Three classes of disulfide-constrained peptides that antagonize VEGF were identified using phage display of naive peptide libraries. NMR chemical shift mapping reveals that the peptide-binding sites on VEGF overlap with the previously identified receptor-binding sites. Representatives of two of these peptide classes, v108 (class 2) and v107 (class 3), have had their structures determined in complex with the VEGF receptor-binding domain. A crystal structure of the VEGF–v108 complex revealed that the class 2 peptide binding mode resembles that of an anti-VEGF antibody, while the NMR solution structure of the VEGF–v107 complex indicates that the class 3 peptide binding mode more closely resembles that of the receptor, Flt-1. The v108 peptide binds VEGF at the edge of the receptor-binding site through primarily main-chain interactions; this fact, coupled with the paucity of side-chain mediated interactions makes this peptide a poor candidate for epitope transfer to a small-molecule scaffold. The structure of the VEGF–v107 complex, however, provides new insight into how binding can be achieved at the VEGF receptor-binding site that might be useful for the design of novel, small-molecule inhibitors.

However, the v107 peptide complex buries ∼70% of the total surface area buried in the protein–receptor complex, and has a functional epitope, as determined by alanine-scanning mutagenesis, that is similar in size to that of the receptor complex and predominantly hydrophobic in nature. Due to the hydrophobic nature of the interaction and the relatively large size of the interface, we therefore conclude that minimization and transfer of the v107 VEGF-binding epitope to a small-molecule scaffold, while still maintaining affinity, will also be difficult. Phage display of peptide libraries has thus successfully targeted relevant protein-binding sites on the VEGF surface, and substituted the natural protein scaffolds with significantly smaller-sized peptide scaffolds to achieve binding at these sites, but has not found smaller binding epitopes that might be generally suitable for binding small-molecules.

Acknowledgements

We thank Stephen Russell, Jeffrey Tom, and Andrea Cochran for producing peptides used in these studies, and Bing Li for carrying out binding assays.

References

[1] Y.A. Muller, B. Li, H.W. Christinger, J.A. Wells, B.C. Cunningham and A.M. de Vos, Vascular endothelial growth factor: crystal structure and functional mapping of the kinase domain receptor binding site, *Proc. Natl. Acad. Sci. USA* **94** (1997), 7192–7197.
[2] N. Ferrara, Role of vascular endothelial growth factor in regulation of physiological angiogenesis, *Am. J. Physiol. Cell Physiol.* **280** (2001), C1358–C1366.
[3] J. Folkman, Angiogenesis in cancer, vascular, rheumatoid and other disease, *Nature Med.* **1** (1995), 27–31.
[4] H.F. Dvorak, L.F. Brown, M. Detmar and A.M. Dvorak, Vascular permeability factor/vascular endothelial growth factor, microvascular hyperpermeability, and angiogenesis, *Am. J. Pathol.* **146** (1995), 1029–1039.
[5] N. Ferrara and T. Davis-Smyth, The biology of vascular endothelial growth factor, *Endocr. Rev.* **18** (1997), 4–25.
[6] K.J. Kim, B. Li, J. Winer, M. Armanini, N. Gillett, H.S. Phillips and N. Ferrara, Inhibition of vascular endothelial growth factor-induced angiogenesis suppresses tumour growth in vivo, *Nature* **362** (1993), 841–844.
[7] N. Ferrara and K. Alitalo, Clinical applications of angiogenic growth factors and their inhibitors, *Nat. Med.* **5** (1999), 1359–1364.
[8] L.G. Presta, H. Chen, S.J. O'Connor, V. Chisholm, Y.G. Meng, L. Krummen, M. Winkler and N. Ferrara, Humanization of an anti-vascular endothelial growth factor monoclonal antibody for the therapy of solid tumors and other disorders, *Cancer Res.* **57** (1997), 4593–4599.
[9] K.A. Houck, D.W. Leung, A.M. Rowland, J. Winer and N. Ferrara, Dual regulation of vascular endothelial growth factor bioavailability by genetic and proteolytic mechanisms, *J. Biol. Chem.* **267** (1992), 26 031–26 037.
[10] R.G. Keck, L. Berleau, R. Harris and B.A. Keyt, Disulfide structure of the heparin binding domain in vascular endothelial growth factor: characterization of posttranslational modifications in VEGF, *Arch. Biochem. Biophys.* **344** (1997), 103–113.
[11] B.A. Keyt, H.V. Nguyen, L.T. Berleau, C.M. Duarte, J. Park, H. Chen and N. Ferrara, Identification of vascular endothelial growth factor determinants for binding KDR and FLT-1 receptors. Generation of receptor-selective VEGF variants by site-directed mutagenesis, *J. Biol. Chem.* **271** (1996), 5638–5646.
[12] C. Wiesmann, G. Fuh, H.W. Christinger, C. Eigenbrot, J.A. Wells and A.M. de Vos, Crystal structure at 1.7 Å resolution of VEGF in complex with domain 2 of the Flt-1 receptor, *Cell* **91** (1997), 695–704.
[13] G. Fuh, B. Li, C. Crowley, B. Cunningham and J.A. Wells, Requirements for binding and signaling of the kinase domain receptor for vascular endothelial growth factor, *J. Biol. Chem.* **273** (1998), 11 197–11 204.
[14] B. Li, G. Fuh, G. Meng, X. Xin, M.E. Gerritsen, B. Cunningham and A.M. de Vos, Receptor-selective variants of human vascular endothelial growth factor. Generation and characterization, *J. Biol. Chem.* **275** (2000), 29 823–29 828.
[15] B.I. Terman, M. Dougher-Vermazen, M.E. Carrion, D. Dimitrov, D.C. Armellino, D. Gospodarowicz and P. Bohlen, Identification of the KDR tyrosine kinase as a receptor for vascular endothelial cell growth factor, *Biochem. Biophys. Res. Commun.* **187** (1992), 1579–1586.
[16] H. Gille, J. Kowalski, B. Li, J. LeCouter, B. Moffat, T.F. Zioncheck, N. Pelletier and N. Ferrara, Analysis of biological effects and signaling properties of Flt-1 (VEGFR-1) and KDR (VEGFR-2), *J. Biol. Chem.* **276** (2001), 3222–3230.
[17] C. de Vries, J.A. Escobedo, H. Ueno, K. Houck, N. Ferrara and L.T. Williams, The fms-like tyrosine kinase, a receptor for vascular endothelial growth factor, *Science* **255** (1992), 989–991.
[18] J.E. Park, H.H. Chen, J. Winer, K.A. Houck and N. Ferrara, Placenta growth factor. Potentiation of vascular endothelial growth factor bioactivity, in vitro and in vivo, and high affinity binding to Flt-1 but not to Flk-1/KDR, *J. Biol. Chem.* **269** (1994), 25 646–25 654.
[19] S. Hiratsuka, O. Minowa, J. Kuno, T. Noda and M. Shibuya, Flt-1 lacking the tyrosine kinase domain is sufficient for normal development and angiogenesis in mice, *Proc. Natl. Acad. Sci. USA* **95** (1998), 9349–9354.
[20] Y.A. Muller, Y. Chen, H.W. Christinger, B. Li, B.C. Cunningham, H.B. Lowman and A.M. de Vos, VEGF and the Fab fragment of a humanized neutralizing antibody: crystal structure of the complex at 2.4 Å resolution and mutational analysis of the interface, *Structure* **6** (1998), 1153–1167.
[21] Y. Chen, C. Wiesmann, G. Fuh, B. Li, H.W. Christinger, P. McKay, A.M. de Vos and H.B. Lowman, Selection and analysis of an optimized anti-VEGF antibody: crystal structure of an affinity-matured Fab in complex with antigen, *J. Mol. Biol.* **293** (1999), 865–881.

[22] W.J. Fairbrother, H.W. Christinger, A.G. Cochran, G. Fuh, C.J. Keenan, C. Quan, S.K. Shriver, J.Y.K. Tom, J.A. Wells and B.C. Cunningham, Novel peptides selected to bind vascular endothelial growth factor target the receptor-binding site, *Biochemistry* **37** (1998), 17 754–17 764.
[23] H.B. Lowman, Y.M. Chen, N.J. Skelton, D.L. Mortensen, E.E. Tomlinson, M.D. Sadick, I.C. Robinson and R.G. Clark, Molecular mimics of insulin-like growth factor 1 (IGF-1) for inhibiting IGF-1: IGF-binding protein interactions, *Biochemistry* **37** (1998), 8870–8878.
[24] M.S. Dennis, C. Eigenbrot, N.J. Skelton, M.H. Ultsch, L. Santell, M.A. Dwyer, M.P. O'Connell and R.A. Lazarus, Peptide exosite inhibitors of factor VIIa as anticoagulants, *Nature* **404** (2000), 465–470.
[25] G.R. Nakamura, M.A. Starovasnik, M.E. Reynolds and H.B. Lowman, A novel family of hairpin peptides that inhibit IgE activity by binding to the high-affinity IgE receptor, *Biochemistry* **40** (2001), 9828–9835.
[26] G.R. Nakamura, M.E. Reynolds, Y.M. Chen, M.A. Starovasnik and H.B. Lowman, Stable "zeta" peptides that act as potent antagonists of the high-affinity IgE receptor, *Proc. Natl. Acad. Sci. USA* **99** (2002), 1303–1308.
[27] N.J. Skelton, S. Russell, F. de Sauvage and A.G. Cochran, Amino acid determinants of β-hairpin conformation in erythropoeitin receptor agonist peptides derived from a phage display library, *J. Mol. Biol.* **316** (2002), 1111–1125.
[28] K. Deshayes, M.L. Schaffer, N.J. Skelton, G.R. Nakamura, S. Kadkhodayan and S.S. Sidhu, Rapid identification of small binding motifs with high-throughput phage display: discovery of peptidic antagonists of IGF-1 function, *Chem. Biol.* **9** (2002), 495–505.
[29] W.J. Fairbrother, M.A. Champe, H.W. Christinger, B.A. Keyt and M.A. Starovasnik, ^{1}H, ^{13}C, and ^{15}N backbone assignment and secondary structure of the receptor-binding domain of vascular endothelial growth factor, *Protein Sci.* **6** (1997), 2250–2260.
[30] B. Pan and W.J. Fairbrother, ^{1}H, ^{13}C, and ^{15}N resonance assignment of the vascular endothelial growth factor receptor-binding domain in complex with a receptor-blocking peptide, *J. Biomol. NMR* 22 (2002), 189–190.
[31] C. Spitzfaden, H.-P. Weber, W. Braun, J. Kallen, G. Wider, H. Widmer, M.D. Walkinshaw and K. Wüthrich, Cyclosporin A-cyclophilin complex formation. A model based on X-ray and NMR data, *FEBS Lett.* **300** (1992), 291–300.
[32] Y. Chen, J. Reizer, M.H. Saier, Jr., W.J. Fairbrother and P.E. Wright, Mapping the binding interfaces of the proteins of the bacterial phosphotransferase system, HPr and IIA^{glc}, *Biochemistry* **32** (1993), 32–37.
[33] E.R.P. Zuiderweg, Mapping protein-protein interactions in solution by NMR spectroscopy, *Biochemistry* **41** (2002), 1–7.
[34] C. Wiesmann, H.W. Christinger, A.G. Cochran, B.C. Cunningham, W.J. Fairbrother, C.J. Keenan, G. Meng and A.M. de Vos, Crystal structure of the complex between VEGF and a receptor-blocking peptide, *Biochemistry* **37** (1998), 17 765–17 772.
[35] J. Cavanagh, W.J. Fairbrother, A.G. Palmer, III and N.J. Skelton, *Protein NMR Spectroscopy: Principles and Practice*, Academic Press, San Diego, 1995.
[36] B. Pan, B. Li, S.J. Russell, J.Y.K. Tom, A.G. Cochran and W.J. Fairbrother, Solution structure of a phage-derived peptide antagonist in complex with vascular endothelial growth factor, *J. Mol. Biol.* **316** (2002), 769–787.
[37] S. Spera and A. Bax, Empirical correlation between protein backbone conformation and Cα and Cβ^{13}C nuclear magnetic resonance chemical shifts, *J. Am. Chem. Soc.* **113** (1991), 5490–5492.
[38] D.S. Wishart and B.D. Sykes, The ^{13}C Chemical Shift Index: a simple method for the identification of protein secondary structure using ^{13}C chemical-shift data, *J. Biomol. NMR* **4** (1994), 171–180.
[39] C.M. Santiveri, M. Roci and M.A. Jiménez, $^{13}C_{\alpha}$ and $^{13}C_{\beta}$ chemical shifts as a tool to delineate β-hairpin structures in peptides, *J. Biomol. NMR* **19** (2001), 331–345.
[40] O. Livnah, E.A. Stura, D.L. Johnson, S.A. Middleton, L.S. Mulcahy, N.C. Wrighton, W.J. Dower, L.K. Jolliffe and I.A. Wilson, Functional mimicry of a protein hormone by a peptide agonist: the EPO receptor complex at 2.8 Å, *Science* **273** (1996), 464–471.
[41] O. Livnah, D.L. Johnson, E.A. Stura, F.X. Farrell, F.P. Barbone, Y. You, K.D. Liu, M.A. Goldsmith, W. He, C.D. Krause, S. Pestka, L.K. Jolliffe and I.A. Wilson, An antagonist peptide–EPO receptor complex suggests that receptor dimerization is not sufficient for activation, *Nature Struct. Biol.* **5** (1998), 993–1003.
[42] S.J. Russell and A.G. Cochran, Designing stable β-hairpins: energetic contributions from cross-strand residues, *J. Am. Chem. Soc.* **122** (2000), 12 600–12 601.
[43] A.G. Cochran, R.T. Tong, M.A. Starovasnik, E.J. Park, R.S. McDowell, J.E. Theaker and N.J. Skelton, A minimal peptide scaffold for β-turn display: optimizing a strand position in disulfide-cyclized β-hairpins, *J. Am. Chem. Soc.* **123** (2001), 625–632.
[44] S.J. Russell, T. Blandl, N.J. Skelton and A.G. Cochran, Stability of cyclic β-hairpins: energetic contributions from hydrogen-bonded cross-strand pairs, *Protein Sci.* (2003) in press.
[45] G. Cornilescu, F. Delaglio and A. Bax, Protein backbone angle restraints from searching a database for chemical shift and sequence homology, *J. Biomol. NMR* **13** (1999), 289–302.
[46] C. Zwahlen, P.L. Sébastien, J.F. Vincent, J. Greenblatt, R. Konrat and L.E. Kay, Methods for measurement of intermolecular NOEs by multinuclear NMR spectroscopy: application to a bacteriophage N-peptide/boxB RNA complex, *J. Am. Chem. Soc.* **119** (1997), 6711–6721.

[47] N. Tjandra and A. Bax, Direct measurement of distances and angles in biomolecules by NMR in a dilute liquid crystalline medium, *Science* **278** (1997), 1111–1114.
[48] J. Kuszewski, J. Qin, A.M. Gronenborn and G.M. Clore, The impact of direct refinement against $^{13}C^{\alpha}$ and $^{13}C^{\beta}$ chemical shifts on protein structure determination by NMR, *J. Magn. Reson. B* **106** (1995), 92–96.
[49] M. Nilges, A calculation strategy for the structure determination of symmetric dimers by ^{1}H NMR, *Proteins* **17** (1993), 297–309.
[50] E.G. Stein, L.M. Rice and A.T. Brünger, Torsion-angle molecular dynamics as a new efficient tool for NMR structure calculation, *J. Magn. Reson.* **124** (1997), 154–164.
[51] Y.A. Muller, H.W. Christinger, B.A. Keyt and A.M. de Vos, The crystal structure of vascular endothelial growth factor (VEGF) refined to 1.93 Å resolution: multiple copy flexibility and receptor binding, *Structure* **5** (1997), 1325–1338.
[52] M.R. Hansen, L. Mueller and A. Pardi, Tunable alignment of macromolecules by filamentous phage yields dipolar coupling interactions, *Nature Struct. Biol.* **5** (1998), 1065–1074.
[53] M. Ottiger, F. Delaglio and A. Bax, Measurement of *J* and dipolar couplings from simplified two-dimensional NMR spectra, *J. Magn. Reson.* **131** (1998), 373–378.
[54] N. Tjandra, J.G. Omichinski, A.M. Gronenborn, G.M. Clore and A. Bax, Use of dipolar ^{1}H–^{15}N and ^{1}H–^{13}C couplings in the structure determination of magnetically oriented macromolecules in solution, *Nature Struct. Biol.* **4** (1997), 732–738.
[55] D.M. Eckert, V.N. Malashkevich, L.H. Hong, P.A. Carr and P.S. Kim, Inhibiting HIV-1 entry: discovery of D-peptide inhibitors that target the gp41 coiled-coil pocket, *Cell* 99 (1999), 103–115.
[56] N.J. Skelton, Y.M. Chen, N. Dubree, C. Quan, D.Y. Jackson, A. Cochran, K. Zobel, K. Deshayes, M. Baca, M.T. Pisabarro and H.B. Lowman, Structure–function analysis of a phage display-derived peptide that binds to insulin-like growth factor binding protein 1, *Biochemistry* **40** (2001), 8487–8498.
[57] R. Koradi, M. Billeter and K. Wüthrich, MOLMOL: a program for display and analysis of macromolecular structures, *J. Mol. Graphics* **14** (1996), 51–55.